ACS APPLIED MATERIALS & INTERFACES

Research Article

Cite This: ACS Appl. Mater. Interfaces 2019, 11, 27453−27463

www.acsami.org

# An Insulating $Al_2O_3$ Overlayer Prevents Lateral Hole Hopping Across Dye-Sensitized $TiO_2$ Surfaces

Matthew D. Brady, Ludovic Troian-Gautier, Tyler C. Motley, Michael D. Turlington, and Gerald J. Meyer*

Department of Chemistry, University of North Carolina at Chapel Hill, Murray Hall 2202B, Chapel Hill, North Carolina 27599-3290, United States

Supporting Information

**ABSTRACT:** Three chromophores of the general form $[Ru(bpy')_2(4,4'\text{-}(PO_3H_2)_2\text{-}2,2'\text{-bipyridine})]^{2+}$, where bpy′ is 4,4′-$(C(CH_3)_3)_2$-2,2′-bipyridine ($Ru(dtb)_2P$); 4,4′-$(CH_3O)_2$-2,2′-bipyridine ($Ru(OMe)_2P$), and 2,2′-bipyridine (RuP) were anchored to mesoporous thin films of $TiO_2$ nanocrystallites at saturation surface coverages to investigate lateral self-exchange $Ru^{III/II}$ intermolecular hole hopping in 0.1 M $LiClO_4$/$CH_3CN$ electrolytes. Hole hopping was initiated by a potential step 500 mV positive of the $E_{1/2}$ ($Ru^{III/II}$) potential or by pulsed laser (532 nm, 8 ns fwhm) excitation and monitored by visible absorption chronoabsorptometry and time-resolved absorption anisotropy measurements, respectively. The hole hopping rate constant $k_R$ extracted from the potential step data revealed self-exchange rate constants that followed the trend: $TiO_2|Ru(OMe)_2P$ ($k_{et} = 1.4 \times 10^6\ s^{-1}$) > $TiO_2|$RuP ($7.1 \times 10^5\ s^{-1}$) > $TiO_2|Ru(dtb)_2P$ ($6.5 \times 10^4\ s^{-1}$). Analysis of the anisotropy data with Monte Carlo simulations provided hole hopping rate constants for $TiO_2|$RuP and $TiO_2|Ru(dtb)_2P$ that were within experimental error the same as that measured with the potential step. The hole hopping rate constants were found to trend with the $TiO_2(e^-)|Ru^{III} \rightarrow TiO_2|Ru^{II}$ charge recombination rate constants. The atomic layer deposition of an ∼10 Å layer of $Al_2O_3$ on top of the dye-sensitized films was found to prevent hole hopping by both initiation methods even though the chromophore surface coverage exceeded the percolation threshold and excited-state injection was efficient. The dramatic hole hopping turnoff was attributed to a larger outer-sphere reorganization energy for self-exchange due to the restricted access of electrolyte to the redox active chromophores. The implications of these findings for solar energy conversion applications are discussed.

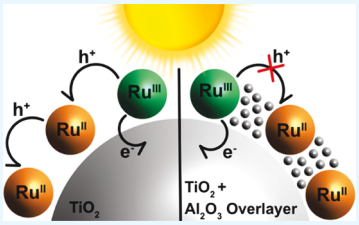


**KEYWORDS:** *dye-sensitized, ruthenium polypyridyl, anisotropy, hole hopping, lateral self-exchange*

## INTRODUCTION

Storage of solar energy in chemical bonds through the photocatalytic conversion of inexpensive and abundant feedstocks to what have been termed "solar fuels" represents a promising strategy.[1−10] One approach to solar fuel production is the dye-sensitized photoelectrosynthesis cell that utilizes wide band gap semiconducting metal oxide nanocrystallites interconnected in a mesoporous thin film with surface-anchored dyes and catalysts.[11−14] In this approach, the excited state of the chromophore injects charge into the semiconductor and then subsequently transfers a redox equivalent to the catalyst that ultimately drives the multielectron transfer reactions necessary for solar fuel production.[15] Dye-sensitized photoelectrosynthesis cells for splitting water[16−18] or hydrohalic acids[19−21] have been reported as well as for $CO_2$ reduction.[22] In some of these reports, the chromophore and catalyst were covalently linked, providing an intramolecular transfer pathway for the redox equivalents.[15,23] In others, the chromophore and catalyst were coanchored to the same surface and the redox equivalents were hence transferred intermolecularly.[24−26] Although the coanchored assembly of chromophores and catalysts is often more straightforward, it was recently shown that the same intermolecular pathways that activate the catalyst can also provide a pathway for unwanted charge recombination reactions.[27] In this report, insulating oxide overlayers are shown to be a useful tool for controlling lateral intermolecular electron transfer that is often called hole hopping.

After excited-state injection into anatase $TiO_2$, it was often thought that the oxidizing equivalent remained fixed at the injection site.[28] Time-resolved absorption anisotropy measurements later showed that this was not the case.[27,29,30] An anisotropic subpopulation of oxidizing equivalents, or holes, can be generated by photoselection of the randomly oriented chromophores on nanocrystallites with linearly polarized light. In the absence of chromophore or nanoparticle diffusion, as is the case with sintered nanoparticles and surface-bound chromophores, the anisotropic distribution should experience little change. However, when chromophores undergo hole hopping across the surface of the nanocrystallites, polarization-dependent absorbance changes can reveal anisotropy decays, which provides information on the self-exchange dynamics across the nanocrystallite surface. These studies revealed that

Received: May 8, 2019
Accepted: July 1, 2019
Published: July 1, 2019






DOI: 10.1021/acsami.9b08051
ACS Appl. Mater. Interfaces 2019, 11, 27453−27463

**Scheme 1. Hole Hopping Mechanisms on $TiO_2$ Nanocrystallites**[a]

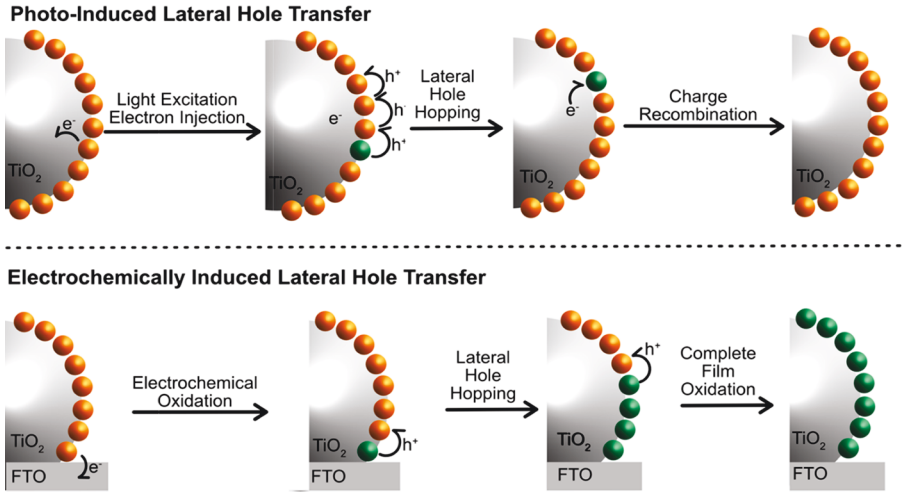


[a]The top panel shows lateral hole hopping between an oxidized (green) and ground-state chromophore (orange) after excited-state injection into $TiO_2$. The lower panel shows that a potential applied to the fluorine-doped tin oxide (FTO) substrate of a saturation surface coverage mesoporous thin film in a standard electrochemical cell can result in complete oxidation of all chromophores within the film by lateral hole hopping.

the oxidizing equivalent can be transported laterally by hole hopping, Scheme 1 (top panel).

Related hole hopping processes have been initiated with an applied potential in a standard electrochemical cell,[31] as shown in Scheme 1 (lower panel). Remarkably, all chromophores within the mesoporous thin film can be reversibly oxidized provided that the surface coverage exceeds a percolation threshold of about 60% of the saturation value.[31−33] An advantage of hole hopping is that it provides a means for transporting charge without loss in free energy. Hole hopping has been exploited to transfer redox equivalents directly to the counter electrode in dye-sensitized solar cells that do not contain a redox mediator[34] and for activation of water oxidation catalysts.[29] Hole hopping has also been found to be deleterious in some cases. Chromophores that participated in fast hole hopping recombined with injected electrons more rapidly, presumably because hole hopping enhanced encounters between the oxidized chromophore and the injected electron.[27,35−37] In addition, the activation of a water oxidation catalyst to the Ru(IV)═O state only occurred when the chromophore surface coverage was below the percolation threshold for hole hopping. At higher surface coverages, the high valent metal oxo Ru(IV)═O was not produced due to charge recombination mediated by lateral hole hopping reactivity.[23] Hence, there is good reason to identify the factors that control hole hopping, particularly at anatase $TiO_2$ interfaces.

Recently, atomic layer deposition (ALD) of insulating oxide overlayers has emerged as a powerful technique to inhibit desorption of molecular chromophores and catalysts from metal oxide surfaces.[38−44] The enhanced stabilization is particularly noteworthy under neutral and alkaline aqueous conditions. Interestingly, the chromophores buried under the oxide overlayers are known to inject electrons into $TiO_2$ when illuminated with light.[39,44] Previous results had demonstrated a decrease in the electrochemical diffusion rate with increasing ALD overlayer thickness.[38] However, a direct comparison between the effects of overlayers on photo- and electrochemically induced hole hopping had not been explored previously.

Herein, a series of three $Ru^{II}$ polypyridyl chromophores surface-immobilized on mesoporous $TiO_2$ nanocrystallite thin films were investigated with and without $Al_2O_3$ overlayers, as shown in Scheme 2. These chromophores were chosen for

**Scheme 2. Three $Ru^{II}$ Chromophore Structures that Differed Only in the Substituents in the 4 and 4′ Positions**[a]

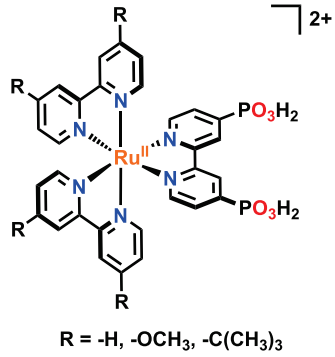


[a]When R = H, the chromophore was abbreviated as RuP, R = $OCH_3$ was likewise $Ru(OMe)_2P$, and R = $C(CH_3)_3$ was $Ru(dtb)_2P$. Note that when these chromophores were anchored to $TiO_2$, this was abbreviated with |, i.e., $TiO_2$|RuP, and the abbreviation when an oxide overlayer was present was $TiO_2$|RuP|$Al_2O_3$.

their high molar absorption coefficient absorption bands in the visible region, high excited-state injection yields, tunable formal reduction potentials competent for mediated water oxidation, high stability in adjacent redox states, and known self-exchange behavior.[45,46] Systematic studies of hole hopping were conducted with chronoabsorptometry and transient anisotropy measurements. It was revealed that the insulating overlayers inhibited potential- and light-induced hole hopping but still allowed for excited-state electron injection.

## EXPERIMENTAL SECTION

**Materials.** The following solvents and reagents were obtained from the indicated commercial suppliers and used without further purification: acetonitrile ($CH_3CN$, Burdick and Jackson, Spectrophotometric grade), lithium perchlorate ($LiClO_4$, Sigma-Aldrich,


DOI: 10.1021/acsami.9b08051
ACS Appl. Mater. Interfaces 2019, 11, 27453−27463

99.99%), methanol ($CH_3OH$, Fisher, Optima), perchloric acid ($HClO_4$, Alfa Aesar, 70%), titanium(IV) isopropoxide ($Ti(i\text{-}OPr)_4$, Aldrich, ≥97.0%), trimethylaluminum (TMA, 97%, Sigma-Aldrich), fluorine-doped tin(IV) oxide-coated glass (FTO, Hartford Glass Co., Inc., 2.3 mm thick 15 Ω/sq), nitrogen ($N_2$, Airgas, Ultra High Purity), oxygen ($O_2$, Airgas, ≥99.998%), and argon (Ar, Airgas, ≥99.999%). All other reagents and solvents were ACS grade and used without additional purification. The chromophores utilized were available from previous studies:[46] $[Ru(bpy')_2(4,4'\text{-}(PO_3H_2)_2\text{-}2,2'\text{-bipyridine})]^{2+}$, where bpy′ is 4,4′-$(C(CH_3)_3)_2$-2,2′-bipyridine ($Ru(dtb)_2P$); 4,4′-$(CH_3O)_2$-2,2′-bipyridine ($Ru(OMe)_2P$), and 2,2′-bipyridine (RuP).

*Sensitized Metal Oxide Thin Film.* Transparent $TiO_2$ nanocrystallites (anatase, ∼20 nm in diameter) were prepared by hydrolysis of $Ti(i\text{-}OPr)_4$ using a previously described sol−gel technique.[47,48] Mesoporous thin films were prepared by doctor blading on a methanol-cleaned FTO glass substrate using Scotch tape (∼50 μm thick) as a spacer to ensure uniform thickness. The doctor-bladed films were covered and allowed to dry at room temperature for 30 min, then sintered under an $O_2$ atmosphere (∼1 atm) for 30 min at 450 °C, resulting in ∼3 μm thick films. These films were stored in a ∼70 °C oven until use.

The thin films were placed into ∼1 mM aqueous chromophore solutions with 0.1 M $HClO_4$ (aq) to allow for surface functionalization. Films reacted for at least 48 h to ensure that uniform, saturation surface coverages were achieved. Prior to use, films were rinsed with neat $CH_3CN$, then soaked in 0.1 M $LiClO_4$ $CH_3CN$ solution for at least 1 h to remove any weakly adsorbed molecules from the surface.

*Atomic Layer Deposition.* Atomic layer deposition (ALD) was performed in a commercial reactor (Savannah S200, Cambridge Nanotech). Aluminum oxide ($Al_2O_3$) was deposited using trimethylaluminum (TMA). The reactor temperature was held at 130 °C, whereas the TMA reservoir was kept at room temperature. The TMA was pulsed into the reactor for 0.02 s and then held for 30 s before opening the pump valve and purging for 35 s. ALD coating conditions were 130 °C with a 20 sccm $N_2$ carrier gas flow rate with a sequence of 0.02 s TMA dose, 30 s hold, 35 s $N_2$ purge, 0.02 s $H_2O$ dose, 30 s hold, 35 s $N_2$ purge for 10 cycles, with ∼1.1 Å $Al_2O_3$ deposited per cycle.[49]

**Spectroscopy.** *UV−Visible Absorption.* All steady-state UV−visible spectra were obtained on an Agilent Cary 60 spectrophotometer at room temperature in 1.0 cm path length glass cuvettes with the functionalized thin films placed along the diagonal at a 45° angle to the incident probe light.

*Nanosecond Transient Anisotropy.* Nanosecond transient anisotropy measurements were obtained with an apparatus similar to that previously described.[50] Briefly, samples were pumped with a Q-switched, pulsed Nd:YAG laser [Quantel USA (BigSky) Brilliant B; 5−6 ns full width at half-maximum, 1 Hz, ∼10 mm in diameter] directed 45° to the film surface and tuned to 532 nm light with the appropriate nonlinear optics. A 150 W xenon arc lamp (Applied Photophysics) served as the probe and was aligned orthogonal to the laser pump excitation light. The probe was directed through a 1/4 m monochromator (Spectral Energy Corp., GM 252) before arriving at the sample. For detection on sub-100 μs time scales, the lamp was pulsed with 100 V at 1 Hz. Detection was achieved in a T format with a monochromator (Spex 1702/04) optically coupled to a R928 photomultiplier tube (Hamamatsu). Transient data were acquired on a computer-interfaced digital oscilloscope (LeCroy 9450, Dual 350 MHz). The instrument response was ∼10 ns. Typically, 60 laser pulses were averaged at each observation wavelength and 5−10 identical measurements were taken and averaged to help increase the signal-to-noise ratio of the anisotropy data.

All measurements utilized a Glan−Taylor polarizer (Thorlabs, GL 10-A) for the excitation light before the sample ($P_{ex}$) and a second Glan−Taylor polarizer ($P_{det}$) for the probe beam. For anisotropy measurements, $P_{ex}$ was set to vertical, the same polarization as the laser, and $P_{det}$ was set to either vertical ($V$) or horizontal ($H$). Magic angle and anisotropy values were calculated via eqs 1 and 2,[30] respectively

$$\Delta Abs_{magic\ angle} = \frac{(VV + 2VH)}{3} \quad (1)$$

$$r = \frac{(VV - VH)}{3\Delta Abs_{magic\ angle}} \quad (2)$$

where $VY$ is the change in absorbance observed with excitation polarization $V$ and detection polarization $Y = V$ or $H$ and $r$ is the anisotropy value.

**Chronoabsorptometry.** Chronoabsorptometry was performed using a BASi Epsilon potentiostat coupled to an Agilent Cary 60 spectrophotometer. A standard three-electrode setup was used with the functionalized thin films as the working electrode, a Pt mesh counter electrode, and an Ag/AgCl pseudoreference electrode. A nonaqueous Ag/AgCl pseudoreference electrode (Pine Research Instrumentation, Inc., AKREF0033) was filled with 0.1 M $LiClO_4$/$CH_3CN$ solution, and the applied potential was referenced to the $E_{1/2}$ ($Ru^{III/II}$) of the surface-bound chromophore. To quantify $D_{CA}$, the absorbance at the metal-to-ligand charge-transfer (MLCT) maximum was monitored while a potential of $E_{1/2}$ ($Ru^{III/II}$) + 500 mV was applied, with data points collected every 12.5 ms. All chronoabsorptometry studies were performed in a 0.1 M $LiClO_4$/$CH_3CN$ solution.

**Computation.** *Data Analysis.* Data fitting was performed in OriginPro 2017, with least-squares error minimization achieved using the Levenberg−Marquardt method. The errors reported for fitting parameters are the standard errors.

*Simulations of Anisotropy Data.* Monte Carlo simulations were employed to simulate the random-walk anisotropy decay observed after vertically polarized light excitation. The simulation utilized a 20 nm spherical nanocrystallite with chromophores spaced at approximately the intermolecular distance, $\delta$, extracted from surface coverage ($\Gamma_0$) measurements, vide infra. The simulated chromophores were distributed across the surface of the sphere through an iterative Coulomb's law force minimization, which produced a nearly even chromophore distribution. To simulate the low laser power utilized experimentally,[36] one hole was generated per nanocrystallite for each simulation. The probability of an initial hole being generated at a specific location was proportional to $\cos^2\varphi$, where $\varphi$ is the inclination angle of the vertical plane, i.e., vertically polarized light has $\varphi = 0$. For each initialization, the excited-state chromophore generated after vertically polarized excitation was assumed to quantitatively inject an electron. After formation of the oxidized chromophore, or hole, a random-walk simulation was performed. For each chromophore, 10 000 random walks consisting of 1000 iterations were averaged to determine the simulated anisotropy decay as a function of the iteration step. Self-exchange electron transfer was modeled with an exponential distance dependence for the probability of transfer with $\beta_{transfer} = 1.2$ Å$^{-1}$, as previously determined.[46] The anisotropy, $r$, at any time during the random walk was calculated via eq 3, where $\langle\cos^2\varphi\rangle$ was the average of the square of the cosine of the inclination angle of the position of the hole.

$$r = \frac{3\langle\cos^2\varphi\rangle - 1}{2} \quad (3)$$

With the time per iteration step as the only adjustable parameter, the experimentally determined anisotropy decays were modeled directly with the simulated anisotropy decays. The best fit with respect to time per iteration was then utilized to determine the resulting self-exchange rate constant, $k_{MC}$, for each chromophore. The Monte Carlo simulations were performed with Wolfram Mathematica 11.0.1.0 on a PC running an Intel Core i7-4720HQ CPU at 2.60 GHz.

## RESULTS

The three chromophores were synthesized through a standard microwave procedure consistent with a previous publication.[51] Upon surface binding to $TiO_2$, the chromophores retained their characteristic metal-to-ligand charge-transfer (MLCT) absorption features centered around 460 nm (Figure 1). After



DOI: 10.1021/acsami.9b08051
ACS Appl. Mater. Interfaces 2019, 11, 27453−27463

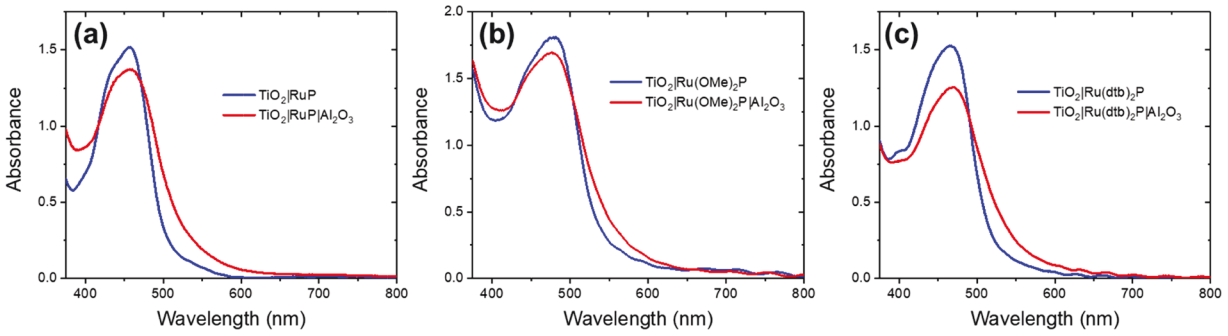


**Figure 1.** Visible absorption spectra of the indicated mesoporous dye-sensitized $TiO_2$ thin films in 0.1 M $LiClO_4/CH_3CN$ for (a) RuP, (b) $Ru(OMe)_2P$, and (c) $Ru(dtb)_2P$ without (blue) and with (red) an $Al_2O_3$ overlayer.

**Table 1. Electrochemical and Photophysical Characterization of $TiO_2|Ru(bpy')_2P$ in $CH_3CN$ Electrolyte**

| chromophore | $\lambda_{MLCT}$ (nm)[a] ($\varepsilon$ $10^4$ $M^{-1}$ $cm^{-1}$) | $E_{1/2}$ ($Ru^{III/II}$)[b] (V vs NHE) | $D_{CA}$ ($10^{-9}$ $cm^2$ $s^{-1}$) | $\Gamma_0$ ($10^{-7}$ mol $cm^{-2}$) | $\delta$ (nm) |
|---|---|---|---|---|---|
| RuP | 458 (1.20) | 1.44 | 2.1 ± 0.2 | 1.3 ± 0.2 | 1.33 ± 0.06 |
| $Ru(OMe)_2P$ | 477 (1.18) | 1.24 | 3.7 ± 0.4 | 1.5 ± 0.1 | 1.26 ± 0.03 |
| $Ru(dtb)_2P$ | 460 (1.40) | 1.37 | 0.21 ± 0.03 | 1.1 ± 0.1 | 1.40 ± 0.07 |

[a]Measured for chromophores dissolved in fluid 0.1 M $HClO_4$ (aq). [b]Ref 46.

10 cycles of $Al_2O_3$ were deposited by atomic layer deposition (ALD), the absorption features were largely preserved, with some broadening of the absorption band displayed beyond 500 nm, as has been previously observed.[39,41] Herein, the oxide interfaces are abbreviated with |; for example, RuP anchored to $TiO_2$ is abbreviated $TiO_2|RuP$, and if an $Al_2O_3$ overlayer is present, $TiO_2|RuP|Al_2O_3$.

The surface coverage, $\Gamma_0$, was calculated from eq 4, where $A_{MLCT}$ is the absorbance maximum measured at the corresponding wavelength, $\lambda_{MLCT}$, and $\varepsilon_{MLCT}$ is the molar extinction coefficient ($M^{-1}$ $cm^{-1}$), which was assumed to retain its value after surface binding. The results are summarized in Table 1.

$$A_{MLCT} = 1000 \times \Gamma_0 \times \varepsilon_{MLCT} \quad (4)$$

To investigate self-exchange hole hopping rates, chronoabsorptometry experiments were conducted utilizing a 100 mM $LiClO_4/CH_3CN$ electrolyte solution. In these experiments, an applied potential step 500 mV more positive than the chromophore $E_{1/2}$ ($Ru^{III/II}$) potential was applied while the spectral changes were monitored as a function of time. Kinetics were monitored at the $\lambda_{MLCT}$ and were plotted as the normalized absorbance change, $\Delta A$, versus the square root of time, $t^{1/2}$. Typical data is shown in Figure 2. Absorbance decreases were observed, consistent with oxidation of the surface-bound chromophores. These data were fit to the Anson equation (eq 5), where $D_{CA}$ is the apparent diffusion coefficient and $d$ is the film thickness. The Anson equation was previously derived using semi-infinite diffusion boundary conditions for molecules undergoing diffusion at electrode surfaces.[31,32,45] Here, because the chromophores are bound to $TiO_2$ thin films of a finite thickness, the data deviate from the predicted linear relationship. However, previous results have shown that a linear relationship is maintained for approximately the first 60% of the total absorbance change.[31,32,45] Therefore, only the first 60% of the total absorbance change was fit, as shown in Figure 2.

$$\Delta A_{MLCT} = \frac{2D_{CA}^{1/2}t^{1/2}}{d\pi^{1/2}} \quad (5)$$

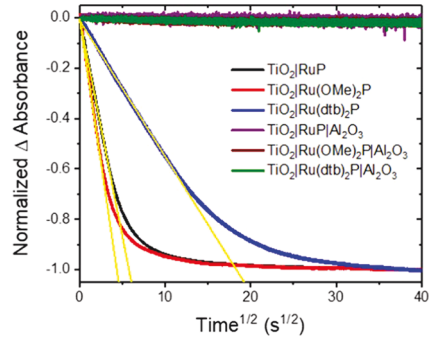


**Figure 2.** Absorption changes monitored at the MLCT absorption maximum after an applied potential step 500 mV more positive than the chromophore $E_{1/2}$ ($Ru^{III/II}$) potential with and without an $Al_2O_3$ overlayer. Overlaid in yellow are fits to the Anson equation (eq 5).

Remarkably, for the sensitized thin films with the ALD $Al_2O_3$ overlayer, no significant absorption changes attributed to chromophore oxidation were observed upon application of potentials sufficient to oxidize the chromophores (Figure 2).

Conversion of the measured diffusion coefficients to a first-order self-exchange "hopping" rate constant, $k_R$, required an estimation of the intermolecular distance, $\delta$, between the chromophores on the surface. It was assumed that the chromophores were evenly distributed within the pore volume of the $TiO_2$ thin film from the measured $\Gamma_0$. The "concentration," $c_0$, was determined using eq 5, where $\Gamma_0 \times 10^4$ is the surface coverage converted to concentration in mol $cm^{-3}$, $N$ is Avogadro's number, $d$ is the film thickness, and $p$ is the porosity, which was assumed to be 60%.[52] This $c_0$ concentration was then converted to an intermolecular distance with the assumption that the chromophores were in a cubic lattice arrangement using $\delta = (c_0)^{-1/3}$, as has been previously done;[45,46,53] see eq 6. With the $\delta$ value, $k_R$ was calculated for each chromophore using the Dahms–Ruff relation,[33,45,54] eq 7. The results are summarized in Table 1 with $k_R$ found in Table 2.



DOI: 10.1021/acsami.9b08051
ACS Appl. Mater. Interfaces 2019, 11, 27453–27463

$$c_0 = \frac{(\Gamma_0 \times 10^4) \times N}{d \times p} \quad (6)$$

$$D_{CA} = \frac{k_R \delta^2}{6} \quad (7)$$

**Table 2. Calculated Rate Constants and Hole-Transfer Correlation Times**

| chromophore | $k_{MA}$ ($s^{-1}$)[a] | $k_{MC}$ ($10^5$ $s^{-1}$) | $k_R$ ($10^5$ $s^{-1}$) | $\theta_{h+}$ (ms) |
|---|---|---|---|---|
| RuP | 5000 | 7 ± 2 | 7.1 ± 0.7 | 2.3 |
| $Ru(OMe)_2P$ | 44 000 | 5 ± 1 | 14 ± 1 | 1.3 |
| $Ru(dtb)_2P$ | 420 | 0.5 ± 0.1 | 0.65 ± 0.06 | 4.0 |

[a] $k_{MA} = 1/\tau$ from eq 9.

Nanosecond transient absorption anisotropy measurements were performed after vertically polarized 532 nm pulsed-light excitation (500 $\mu$J/pulse) on $TiO_2$ thin films sensitized to saturation surface coverage with each chromophore with and without an $Al_2O_3$ overlayer. Immediate bleaching of the MLCT absorption band was observed, consistent with instrument response limited electron injection, $k_{inj} > 10^8$ $s^{-1}$, from the excited state of the chromophore to the $TiO_2$ acceptor states. Kinetics were monitored at 485 nm for $TiO_2$|RuP and $TiO_2$|$Ru(dtb)_2P$ and 510 nm for $TiO_2$|$Ru(OMe)_2P$ with $P_{det}$ set to either vertical ($V$) or horizontal ($H$). Anisotropy was indeed observed for all three chromophores as $VV$ differed significantly from $VH$. Anisotropy decays were evident as the temporal data coalesced beyond 100 $\mu$s for all three chromophores prior to the complete recovery of the bleach.

Sensitized $TiO_2$ thin films with an $Al_2O_3$ overlayer were similarly characterized by time-resolved anisotropy measurements. More rapid recovery of the bleach on time scales <100 ns was also evident for all three chromophores, as well as photoluminescence, consistent with the presence of the MLCT excited-state and nonquantitative excited-state injection. In the absence of an $Al_2O_3$ overlayer, anisotropy decay was present for all three chromophores, whereas in the presence of an $Al_2O_3$ overlayer, anisotropy was independent of time.

The kinetic data were nonexponential under all conditions studied and were instead modeled with the Kohlrausch–Williams–Watts (KWW) stretched exponential function, eq 8, where $A_0$ is the initial amplitude, $k$ is the characteristic rate constant, and $\beta$ is inversely proportional to the width of an underlying Lévy distribution. $\beta$ values in the range of 0.15–0.2 provided the best fit for all decays. A comparison of the kinetic data for $TiO_2$|$Ru(dtb)_2P$ and $TiO_2$|$Ru(dtb)_2P$|$Al_2O_3$ is shown in Figure 3, with the corresponding data for the other chromophores in Figures S1 and S2. A comparison of the initial Δ absorbance amplitudes with $TiO_2$|RuP in 0.1 M $HClO_4$ as an actinometric standard[20,55] indicated an excited-state electron injection quantum yield of ~0.6 when the $Al_2O_3$ overlayer was present.

$$\mathrm{Abs}(t) = A_0 e^{-(kt)^\beta} \quad (8)$$

The resulting fits of $VV$ and $VH$ to the KWW function were substituted into eqs 1 and 2 to calculate the magic angle absorption change (see the SI) and the anisotropy decay, as shown in Figure 4. Note that the minor increase in anisotropy observed at longer times in Figure 4 is likely an artifact that results from the very poor signal-to-noise ratios on the millisecond and longer time scales. The magic angle kinetic data were well-modeled by eq 8. Measurements at the magic angle (Figure S3) provided information on charge recombination of the injected electron and oxidized chromophore, and an average lifetime, $\tau$, was calculated as the first moment of the underlying Lévy distribution in eq 9, where $k$ and $\beta$ are the same from eq 7 and $\Gamma$ is equal to the gamma function. An average rate constant, $k_{MA}$, was taken as the reciprocal of $\tau$, such that $k_{MA} = 1/\tau$. The results are summarized in Table 2.

$$\tau = \frac{1}{k\beta}\Gamma\left(\frac{1}{\beta}\right) \quad (9)$$

The transient absorption data, calculated anisotropy with the resulting Monte Carlo simulation overlaid, and the KWW fit anisotropy data with the Monte Carlo simulation overlaid for RuP are given in Figure 5. The data for the other chromophores are found in Figures S4 and S5. The resulting calculated self-exchange rate constants ($k_{MC}$) for each chromophore are summarized in Table 2.

A rotational hole-transfer correlation time, $\theta$, was determined, which corresponds to the anisotropy loss due to lateral hole hopping across the spherical nanocrystallite, eq 10, where $r(t)$ is the anisotropy as a function of time an $r_0$ is the initial anisotropy. An averaged hole-transfer correlation time, $\theta_{h+}$, was again taken as the first moment of the underlying Lévy distribution, in eq 11. The results are summarized in Table 2 with the overlaid fits in Figure 6.

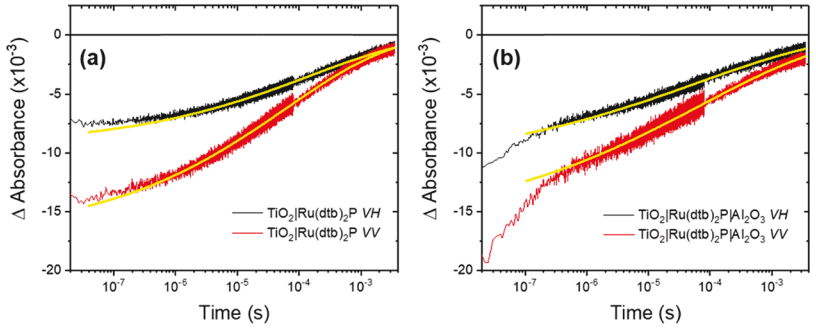


**Figure 3.** Absorption changes monitored at 485 nm after 532 nm pulsed-light excitation (500 $\mu$J/pulse) of $TiO_2$|$Ru(dtb)_2P$ measured with vertical excitation and horizontal ($VH$) or vertical ($VV$) detection without (a) and with (b) an ALD $Al_2O_3$ overlayer. Overlaid in yellow are fits to the KWW function.



DOI: 10.1021/acsami.9b08051
ACS Appl. Mater. Interfaces 2019, 11, 27453–27463

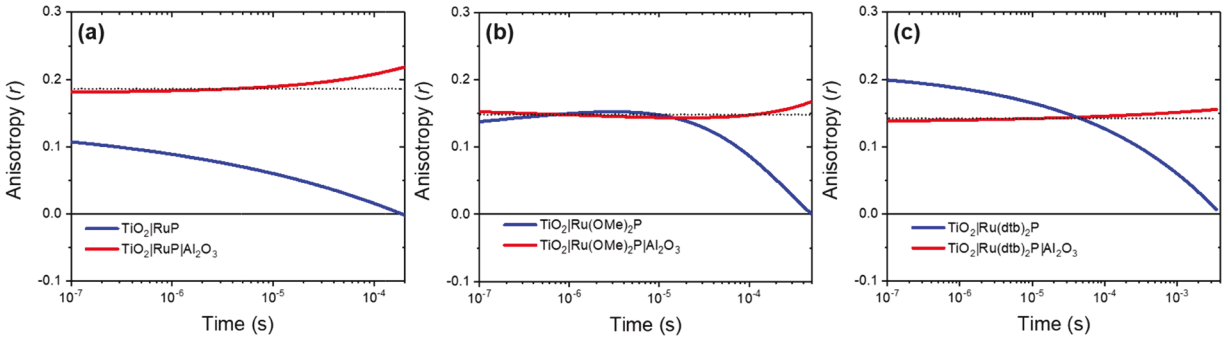


**Figure 4.** Time-dependent anisotropies obtained from fits to the KWW function for (a) RuP, (b) $Ru(OMe)_2P$, and (c) $Ru(dtb)_2P$ without (blue) and with (red) an $Al_2O_3$ overlayer. The black dotted line represents the expected anisotropy when no lateral hole hopping occurs.

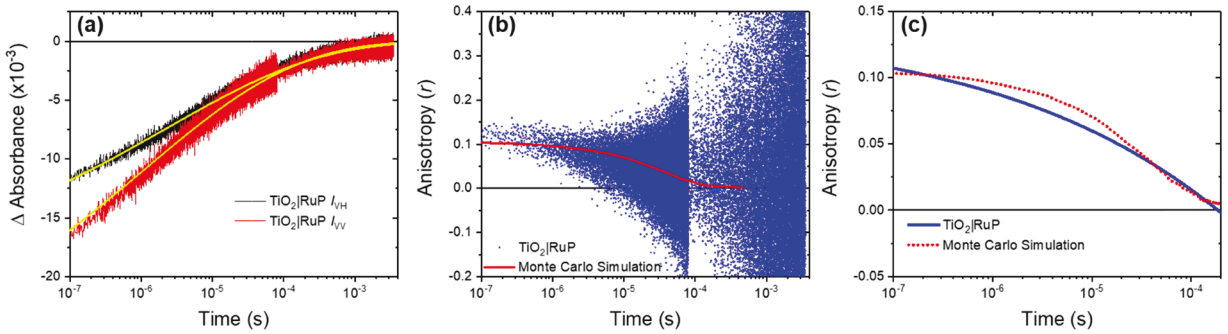


**Figure 5.** (a) Absorption changes monitored at 485 nm after 532 nm pulsed-light excitation (500 $\mu$J/pulse) of $TiO_2$|RuP measured with vertical excitation and horizontal (*VH*) or vertical (*VV*) detection. (b) Experimentally determined anisotropy data with the resultant Monte Carlo simulation overlaid in red. (c) Calculated anisotropy from KWW fits with the Monte Carlo simulation overlaid in red.

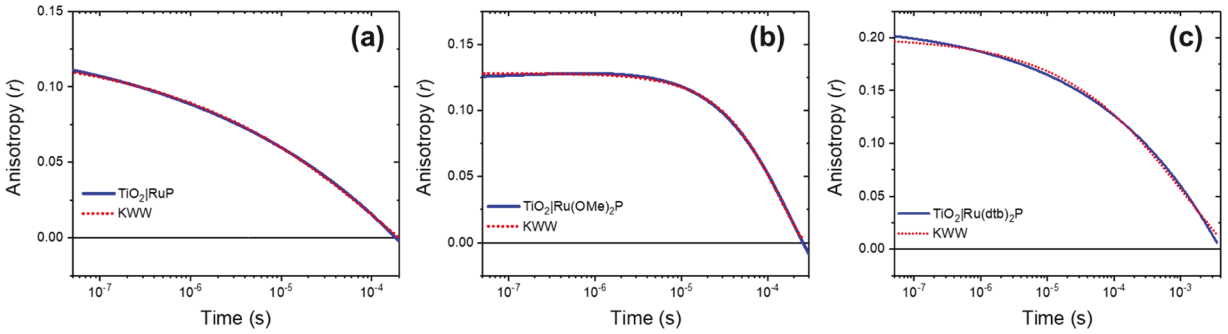


**Figure 6.** Calculated anisotropy traces from KWW fits (blue) with fits to eq 10 overlaid (red) for (a) $TiO_2$|RuP, (b) $TiO_2$|$Ru(OMe)_2P$, and (c) $TiO_2$|$Ru(dtb)_2P$.

$$r(t) = r_0 e^{-(t/\theta)^{\beta_{KWW}}} \quad (10)$$

$$\theta_{h+} = \frac{\theta}{\beta_{KWW}} \Gamma\left(\frac{1}{\beta_{KWW}}\right) \quad (11)$$

## DISCUSSION

Lateral hole hopping, or equivalently intermolecular self-exchange electron transfer, across nanocrystalline oxide surfaces has been shown to be of value to some solar energy conversion schemes and detrimental to others. Kinetic control of hole hopping has been realized to some extent through the introduction of bulky substituents on the redox active molecules,[46] but greater control is needed. In a recent communication, the apparent diffusion coefficient for hole hopping was found to decrease by a factor of 40 when an $Al_2O_3$ overlayer was deposited.[38] The authors suggested that the slower hole hopping resulted from decreased electronic coupling between the chromophores. In this report, it was found that an ~10 Å thick $Al_2O_3$ overlayer dramatically impacts lateral hole hopping with a much smaller impact on the excited-state injection yield. Below, we discuss the observations that led to these conclusions, first with dye-sensitized $TiO_2$ and then with the $Al_2O_3$ overlayer. The discussion concludes with a description of why the overlayer inhibits hole hopping and some speculation as to how it might be exploited for practical energy applications.

**Dye-Sensitized $TiO_2$.** The sensitized $TiO_2$ thin films investigated were typical of those reported in the vast dye-sensitized solar cell literature.[56] Surface coverages of $\sim 1 \times 10^{-7}$ mol/cm$^2$ were measured, values that many interpret as monolayer coverage.[57] When utilized as a working electrode in a standard electrochemical cell with a 100 mM $LiClO_4$/$CH_3CN$ electrolyte, the application of a potential 500 mV


DOI: 10.1021/acsami.9b08051
ACS Appl. Mater. Interfaces 2019, 11, 27453−27463

positive of the chromophore $E_{1/2}$ ($Ru^{III/II}$) value resulted in oxidation of the surface-anchored chromophores. Anson plots of the corresponding absorption change enabled the apparent diffusion constants to be abstracted, $D_{CA}$, which, with some assumptions, provided the self-exchange rate constant for hole hopping, $k_R$. The rate constant $k_R$ decreases from $TiO_2$|$Ru(OMe)_2P$ having the largest ($k_R = 1.4 \times 10^6$ $s^{-1}$), followed by $TiO_2$|RuP ($7.1 \times 10^5$ $s^{-1}$), and $TiO_2$|$Ru(dtb)_2P$ ($6.5 \times 10^4$ $s^{-1}$). The slower hole hopping for $TiO_2$|$Ru(dtb)_2P$ < $TiO_2$|RuP has been previously reported and was attributed to weaker electronic coupling induced by the bulky tertiary butyl groups.[46]

Light excitation of the chromophores in the same electrolyte resulted in excited-state injection with a quantum yield of unity and $k_{inj} > 10^8$ $s^{-1}$, which is consistent with previous literature reports.[58] The excitation light was vertically polarized resulting in an expected preferential creation of oxidized chromophores at the north and south poles of each spherical anatase nanocrystallite in the mesoporous thin film. Observations made with polarizers oriented vertical, *VV* and horizontal, *VH*, to the excitation provided anisotropy decays. A larger absorbance change was measured for *VV*, consistent with an anisotropic distribution of oxidized chromophores. The initial anisotropy was less than the 0.4 value expected theoretically,[59] a behavior which has been observed previously for this class of chromophores in fluid solution and at $TiO_2$ interfaces, which has been attributed to excitation of multiple charge-transfer transitions.[60−62] The transient *VV* and *VH* data coalesced prior to the complete recovery of the ground state, which indicated that the rate constant for hole hopping was greater than that for charge recombination.

Monte Carlo simulations were performed to simulate the expected random-walk nature of isoenergetic, self-exchange hole hopping and to extract self-exchange rate constants, $k_{MC}$. This was accomplished by a previously described method with the assumption of a 20 nm spherical nanocrystal and chromophores arranged at a minimum distance $\delta$ that reflected the slightly different surface coverage measured for each chromophore.[30] With the hopping time as the only adjustable parameter, the measured anisotropy decays were well-modeled by the resulting Monte Carlo simulations. The self-exchange rate constants $k_{MC}$ obtained in this way followed a similar trend as that measured after a potential step: $TiO_2$|RuP having the largest ($k_{MC} = 7 \times 10^5$ $s^{-1}$), followed by $TiO_2$|$Ru(OMe)_2P$ ($5 \times 10^5$ $s^{-1}$), and $TiO_2$|$Ru(dtb)_2P$ ($5 \times 10^4$ $s^{-1}$). It is sometimes useful to consider an average hopping time of $(1.5\ \mu s)^{-1}$, $(2\ \mu s)^{-1}$, and $(20\ \mu s)^{-1}$ for RuP, $Ru(OMe)_2P$, and $Ru(dtb)_2P$, respectively.

Alternatively, in the biophysics fluorescence literature, a correlation time is considered. Fluorescence anisotropy has been widely utilized as a rotational probe in biophysical assays.[59] However, in the case of surface-bound chromophores, it is not rotational diffusion in solution, rather lateral self-exchange translating charge around the spherical nanocrystallite that can be probed through an anisotropy assay. Thus, the average hole-transfer correlation time, $\theta_{h+}$, is taken as the average time for a hole to move one radian from the inclination angle along the surface of the spherical nanocrystal, rather than the time to rotate one radian in solution. The $\theta_{h+}$ values were in good agreement with the calculated electrochemically induced self-exchange rate constants ($k_R$), with smaller $\theta_{h+}$ values: $Ru(OMe)_2P$ ($\theta_{h+}$ = 1.3 ms), RuP (2.3 ms), and $Ru(dtb)_2P$ (4.0 ms), corresponding to larger $k_R$ values.

The values for the self-exchange rate constants obtained by pulsed-light excitation and a potential step were in poor agreement for $TiO_2$|$Ru(OMe)_2P$. However, this chromophore showed the fastest charge recombination rate constants, providing a smaller time period for monitoring hole hopping by anisotropy, which led to a less robust rate constant. On the other hand, the values for $TiO_2$|$Ru(dtb)_2P$ and $TiO_2$|RuP were within reasonable error independent of the method in which the hole hopping was initiated. This is a surprising result in itself. Since the light-initiated reactions reported on self-exchange on a single nanocrystallite and the potential step data reported on hole hopping through the entire mesoporous thin film, one might have anticipated that the values would be quite different. For example, hole hopping at the necking regions between the nanocrystallites might be slower, resulting in vastly different rate constants. As this was not the case, the kinetic data suggests that hole hopping is relatively uniform on a single nanocrystallite and throughout the mesoporous film.

Absorption measurements at the magic angle, which mathematically eliminates anisotropic contributions from the observed absorbance changes, provided kinetic information on $TiO_2(e^-)|Ru^{III} \rightarrow TiO_2|Ru^{II}$ charge recombination. The extracted charge recombination rate constants $k_{MA}$ trend with the hole hopping rate constants. This correlation has previously been reported in the literature with other chromophores where those that underwent the fastest hole hopping also recombined to ground-state products fastest.[36] Taken together, this data indicates that the established mechanism for charge recombination, wherein the oxidized chromophore remains fixed at the injection site and the injected electron alone is mobile, is incorrect. In fact, it may be just the opposite, where the injected electron traps at a localized site and recombination occurs when the oxidized chromophore approaches this site by lateral hole hopping.

**Dye-Sensitized $TiO_2$ with an $Al_2O_3$ Overlayer.** When an insulating $Al_2O_3$ overlayer was deposited on the dye-sensitized $TiO_2$ thin films, there was vanishingly little evidence for hole hopping. Application of an electrochemical bias 500 mV positive of the chromophore $E_{1/2}$ ($Ru^{III/II}$) potential resulted in negligibly small absorbance changes (<5%) attributed to some hole transfer near the fluorine-doped tin oxide (FTO) substrate that supports the mesoporous thin film, even though the chromophores surface coverages greatly exceeded the 50−60% percolation threshold. Although the lack of a significant response to a potential step might be explained by a blocking layer at the FTO interface, transient anisotropy measurements also revealed no evidence for hole hopping. Pulsed-light excitation resulted in significant excited-state injection, which decreased by about 40% from that observed without the insulating overlayer. However, kinetics measured at the magic angle and with polarizers were within the same experimental error and provided no evidence of hole hopping.

The question that then arises is why is lateral hole hopping inhibited with an insulating $Al_2O_3$ overlayer? An unambiguous answer to this question remains unknown, but previous studies of photoinduced electron transfer in rigid media provide a reasonable explanation: the outer-sphere reorganization energy for electron transfer increases when ion and solvent motion are restricted.[63] Indeed, electron transfer quenching is inhibited in the solid state and experiments with a series of porphyrin−quinone complexes revealed that an additional 800 meV of driving force was needed to initiate electron transfer in a frozen glass relative to fluid solution.[64] Photoinduced electron transfer


DOI: 10.1021/acsami.9b08051
ACS Appl. Mater. Interfaces 2019, 11, 27453−27463

in a rigid polymer matrix at room temperature has also shown a similar behavior.[63] Hence, it is likely that the $Al_2O_3$ overlayer inhibits solvent and/or ions from accessing the chromophores, thereby increasing the reorganization energy and preventing hole hopping.

The proposed increase in outer-sphere reorganization energy would not necessarily inhibit excited-state injection because the free-energy change is very different. Hole hopping occurs with $\Delta G^\circ = 0$, whereas excited-state injection is activationless when the excited-state reduction potential is more than twice the reorganization energy above the semiconductor conduction band edge. The ~40% decrease in injection yield may be due to those chromophores where injection does have a barrier. In principle, chromophores that are more potent photoreductants could show excited-state injection yields near unity when the insulating overlayer is present.

**Implications for Practical Solar Energy Conversion Applications.** Uncovering a strategy to allow for photoinduced electron injection from a chromophore without subsequent self-exchange processes is expected to allow for greater site isolation of chromophores and catalysts at the high surface coverages needed for efficient light harvesting. Catalytic reactions like water oxidation require the accumulation of multiple redox equivalents on a catalyst, which often occurs in kinetic competition with unwanted lateral self-exchange-mediated recombination chemistry.[65,66] Although decreasing catalyst surface coverage below percolation thresholds has been shown to inhibit this self-exchange chemistry,[23] this strategy can limit catalysis at high light intensities. Hence, an insulating overlayer may be a promising strategy as it allows for saturation surface coverages that preserve excited-state injection and inhibit unwanted recombination pathways.

An idealized model for how an insulating overlayer could enhanced water oxidation photocatalysis is shown in Scheme 3 with chromophore-catalysts compounds depicted as the orange-blue spheres. Water oxidation requires four oxidizing equivalents to be transferred from the oxidized chromophores.[11] For simplicity, only two oxidations are shown on the catalysts in this simplified schematic and are depicted as green (1+) and pink (2+) spheres. Light absorption results in excited-state injection into $TiO_2$ followed by intramolecular electron transfer from the oxidized chromophore to the catalyst. At saturation surface coverages, lateral hole hopping provides a means to equilibrate all catalysts to a common formal oxidation state. For example, a catalyst in the formal oxidation state of 0 (blue) next to a catalyst in the 2+ (pink) state would reduce it by electron transfer (or hole hopping in the other direction) to generate two catalysts in the 1+ (green) state. When such equilibration is rapid, all of the catalysts would be present on one formal oxidation state or a Nernstian mixture of two states at any given time. It has been previously shown that such a large surface coverage of oxidized catalysts increases the probability for recombination with a $TiO_2$ electron trapped near the surface.[23] In contrast, an insulating overlayer would enable each chromophore-catalyst compound to go through the entire catalytic cycle without equilibration with neighboring compounds. It is important to note that the $Al_2O_3$ overlayer thickness must afford access of the catalyst to the aqueous solution and allow reorganization through all mechanistic steps in the catalytic cycle. Hence, ALD or other deposition techniques must be carefully controlled to prevent lateral hole hopping without deactivation of the catalysts. Future research will test the validity of this approach.

**Scheme 3. Idealized Model Depicting a $TiO_2$ Nanocrystallite with Surface-Anchored Chromophore-Catalyst Compounds**[a]

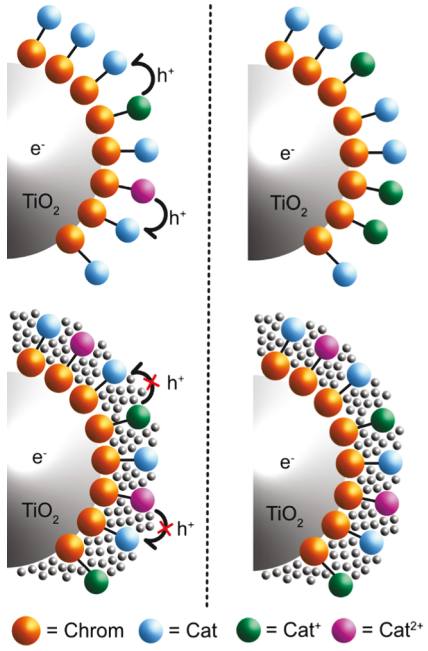


[a]The orange chromophores and blue catalysts, after light excitation, electron injection, and intramolecular electron transfer, result in catalysts that are oxidized by one electron (green spheres). When the same process occurs a second time, catalysts that are oxidized by two electrons are formed (pink spheres). In the absence of an $Al_2O_3$ overlayer (top), hole hopping provides a means for all catalysts to equilibrate to a common oxidation state or a Nernstian mixture of two. Introduction of an $Al_2O_3$ overlayer (bottom) provides site isolation of the catalysts by preventing lateral hole hopping.

## CONCLUSIONS

Three $Ru^{II}$ polypyridyl chromophores anchored to mesoporous $TiO_2$ semiconductor thin films enabled the rate constants for intermolecular self-exchange electron transfer, also called lateral hole hopping, to be quantified after a potential step or pulsed-light excitation. The rate constants extracted from the electrochemical and spectroscopic data were in good agreement for two of the chromophores and showed more sluggish hole hopping when bulky *tert*-butyl substituents were present, consistent with previous results. Monte Carlo simulations revealed average hole hopping rates that ranged between 2 and 20 microseconds per hop. In pulsed-light experiments, more rapid hole hopping also led to faster charge recombination with the injected electron, as has been previously reported.[27] When the sensitized thin films were covered with an $Al_2O_3$ overlayer, the excited-state injection yield decreased from unity to about 0.6; more dramatically, hole hopping was absent. This behavior was attributed to exclusion of the electrolyte from the chromophores by the overlayer which increased the reorganization energy for electron transfer. The results indicate that insulating overlayers provide a potential strategy for site isolation of chromophores or catalysts, where excited-state interfacial electron transfer is largely preserved but unwanted lateral self-exchange electron transfer is inhibited.


DOI: 10.1021/acsami.9b08051
ACS Appl. Mater. Interfaces 2019, 11, 27453−27463

## ■ ASSOCIATED CONTENT

### Supporting Information

The Supporting Information is available free of charge on the ACS Publications website at DOI: 10.1021/acsami.9b08051.

Transient absorption anisotropy, transient absorption, and Monte Carlo simulations (PDF)

## ■ AUTHOR INFORMATION


### Corresponding Author

*E-mail: gjmeyer@email.unc.edu.

### ORCID

Matthew D. Brady: 0000-0002-3917-1072
Ludovic Troian-Gautier: 0000-0002-7690-1361
Tyler C. Motley: 0000-0002-7749-9183
Gerald J. Meyer: 0000-0002-4227-6393


### Notes

The authors declare no competing financial interest.

## ■ ACKNOWLEDGMENTS

This research is supported by the National Science Foundation (NSF) under Award Number 1800022. This work made use of atomic layer deposition instrumentation at the Chapel Hill Analytical and Nanofabrication Laboratory (CHANL), a member of the North Carolina Research Triangle Nanotechnology Network (RTNN), which is supported by the National Science Foundation (Grant ECCS-1542015) as part of the National Nanotechnology Coordinated Infrastructure (NNCI). T.C.M. and M.D.T. would like to acknowledge the NSF Graduate Research Fellowship for support (Grant No. DGE-1144081 and DGE-1650116, respectively).

## ■ REFERENCES


(1) Cogdell, R. J.; Gardiner, A. T.; Yukihira, N.; Hashimoto, H. Solar Fuels and Inspiration from Photosynthesis. *J. Photochem. Photobiol., A* **2018**, *353*, 645−653.

(2) House, R. L.; Iha, N. Y. M.; Coppo, R. L.; Alibabaei, L.; Sherman, B. D.; Kang, P.; Brennaman, M. K.; Hoertz, P. G.; Meyer, T. J. Artificial Photosynthesis: Where Are We Now? Where Can We Go? *J. Photochem. Photobiol., C* **2015**, *25*, 32−45.

(3) Ganesh, I. Solar Fuels Vis-à-Vis Electricity Generation from Sunlight: The Current State-of-the-Art (a Review). *Renew. Sustainable Energy Rev.* **2015**, *44*, 904−932.

(4) Cook, T. R.; Dogutan, D. K.; Reece, S. Y.; Surendranath, Y.; Teets, T. S.; Nocera, D. G. Solar Energy Supply and Storage for the Legacy and Nonlegacy Worlds. *Chem. Rev.* **2010**, *110*, 6474−6502.

(5) McDaniel, N. D.; Bernhard, S. Solar Fuels: Thermodynamics, Candidates, Tactics, and Figures of Merit. *Dalton Trans.* **2010**, *39*, 10021−10030.

(6) Lewis, N. S.; Nocera, D. G. Powering the Planet: Chemical Challenges in Solar Energy Utilization. *Proc. Natl. Acad. Sci. U.S.A.* **2006**, *103*, 15729−15735.

(7) Nocera, D. G. Chemistry of Personalized Solar Energy. *Inorg. Chem.* **2009**, *48*, 10001−10017.

(8) Li, J.; Wu, N. Semiconductor-Based Photocatalysts and Photoelectrochemical Cells for Solar Fuel Generation: A Review. *Catal. Sci. Technol.* **2015**, *5*, 1360−1384.

(9) Walter, M. G.; Warren, E. L.; McKone, J. R.; Boettcher, S. W.; Mi, Q.; Santori, E. A.; Lewis, N. S. Solar Water Splitting Cells. *Chem. Rev.* **2010**, *110*, 6446−6473.

(10) Meyer, T. J. Chemical Approaches to Artificial Photosynthesis. *Acc. Chem. Res.* **1989**, *22*, 163−170.

(11) Brennaman, M. K.; Dillon, R. J.; Alibabaei, L.; Gish, M. K.; Dares, C. J.; Ashford, D. L.; House, R. L.; Meyer, G. J.; Papanikolas, J. M.; Meyer, T. J. Finding the Way to Solar Fuels with Dye-Sensitized Photoelectrosynthesis Cells. *J. Am. Chem. Soc.* **2016**, *138*, 13085−13102.

(12) Yu, Z.; Li, F.; Sun, L. Recent Advances in Dye-Sensitized Photoelectrochemical Cells for Solar Hydrogen Production Based on Molecular Components. *Energy Environ. Sci.* **2015**, *8*, 760−775.

(13) Xu, P.; McCool, N. S.; Mallouk, T. E. Water Splitting Dye-Sensitized Solar Cells. *Nano Today* **2017**, *14*, 42−58.

(14) Grätzel, M. Photoelectrochemical Cells. *Nature* **2001**, *414*, 338−344.

(15) Brennaman, M. K.; Gish, M. K.; Alibabaei, L.; Norris, M. R.; Binstead, R. A.; Nayak, A.; Lapides, A. M.; Song, W.; Brown, R. J.; Concepcion, J. J.; Templeton, J. L.; Papanikolas, J. M.; Meyer, T. J. Pathways Following Electron Injection: Medium Effects and Cross-Surface Electron Transfer in a Ruthenium-Based, Chromophore-Catalyst Assembly on $TiO_2$. *J. Phys. Chem. C* **2018**, *122*, 13017−13026.

(16) Alibabaei, L.; Sherman, B. D.; Norris, M. R.; Brennaman, M. K.; Meyer, T. J. Visible Photoelectrochemical Water Splitting into $H_2$ and $O_2$ in a Dye-Sensitized Photoelectrosynthesis Cell. *Proc. Natl. Acad. Sci. U.S.A.* **2015**, *112*, 5899−5902.

(17) Li, F.; Fan, K.; Xu, B.; Gabrielsson, E.; Daniel, Q.; Li, L.; Sun, L. Organic Dye-Sensitized Tandem Photoelectrochemical Cell for Light Driven Total Water Splitting. *J. Am. Chem. Soc.* **2015**, *137*, 9153−9159.

(18) Sherman, B. D.; Sheridan, M. V.; Wee, K. R.; Marquard, S. L.; Wang, D.; Alibabaei, L.; Ashford, D. L.; Meyer, T. J. A Dye-Sensitized Photoelectrochemical Tandem Cell for Light Driven Hydrogen Production from Water. *J. Am. Chem. Soc.* **2016**, *138*, 16745−16753.

(19) Brady, M. D.; Sampaio, R. N.; Wang, D.; Meyer, T. J.; Meyer, G. J. Dye-Sensitized Hydrobromic Acid Splitting for Hydrogen Solar Fuel Production. *J. Am. Chem. Soc.* **2017**, *139*, 15612−15615.

(20) Brady, M. D.; Troian-Gautier, L.; Sampaio, R. N.; Motley, T. C.; Meyer, G. J. Optimization of Photocatalyst Excited- and Ground-State Reduction Potentials for Dye-Sensitized HBr Splitting. *ACS Appl. Mater. Interfaces* **2018**, *10*, 31312−31323.

(21) Berardi, S.; Cristino, V.; Canton, M.; Boaretto, R.; Argazzi, R.; Benazzi, E.; Ganzer, L.; Borrego Varillas, R.; Cerullo, G.; Syrgiannis, Z.; Rigodanza, F.; Prato, M.; Bignozzi, C. A.; Caramori, S. Perylene Diimide Aggregates on Sb-Doped $SnO_2$: Charge Transfer Dynamics Relevant to Solar Fuel Generation. *J. Phys. Chem. C* **2017**, *121*, 17737−17745.

(22) Wang, D.; Wang, Y.; Brady, M.; Sheridan, M.; Sherman, B. D.; Farnum, B.; Liu, Y.; Marquard, S.; Meyer, G. J.; Dares, C.; Meyer, T. J. A Donor-Chromophore-Catalyst Assembly for Solar $CO_2$ Reduction. *Chem. Sci.* **2019**, 4436−4444.

(23) Hu, K.; Sampaio, R. N.; Marquard, S. L.; Brennaman, M. K.; Tamaki, Y.; Meyer, T. J.; Meyer, G. J. A High-Valent Metal-Oxo Species Produced by Photoinduced One-Electron, Two-Proton Transfer Reactivity. *Inorg. Chem.* **2018**, *57*, 486−494.

(24) Materna, K. L.; Jiang, J.; Regan, K. P.; Schmuttenmaer, C. A.; Crabtree, R. H.; Brudvig, G. W. Optimization of Photoanodes for Photocatalytic Water Oxidation by Combining a Heterogenized Iridium Water-Oxidation Catalyst with a High-Potential Porphyrin Photosensitizer. *ChemSusChem* **2017**, *10*, 4526−4534.

(25) Wang, D.; Marquard, S. L.; Troian-Gautier, L.; Sheridan, M. V.; Sherman, B. D.; Wang, Y.; Eberhart, M. S.; Farnum, B. H.; Dares, C. J.; Meyer, T. J. Interfacial Deposition of Ru(II) Bipyridine-Dicarboxylate Complexes by Ligand Substitution for Applications in Water Oxidation Catalysis. *J. Am. Chem. Soc.* **2018**, *140*, 719−726.

(26) Chen, H. Y.; Ardo, S. Direct Observation of Sequential Oxidations of a Titania-Bound Molecular Proxy Catalyst Generated through Illumination of Molecular Sensitizers. *Nat. Chem.* **2018**, *10*, 17−23.

(27) Moia, D.; Szumska, A.; Vaissier, V.; Planells, M.; Robertson, N.; O'Regan, B. C.; Nelson, J.; Barnes, P. R. F. Interdye Hole Transport Accelerates Recombination in Dye Sensitized Mesoporous Films. *J. Am. Chem. Soc.* **2016**, *138*, 13197−13206.

(28) Nazeeruddin, M. K.; Baranoff, E.; Grätzel, M. Dye-Sensitized Solar Cells: A Brief Overview. *Sol. Energy* **2011**, *85*, 1172−1178.

(29) Ardo, S.; Meyer, G. J. Direct Observation of Photodriven Intermolecular Hole Transfer across $TiO_2$ Nanocrystallites: Lateral Self-Exchange Reactions and Catalyst Oxidation. *J. Am. Chem. Soc.* **2010**, *132*, 9283−9285.
(30) Ardo, S.; Meyer, G. J. Characterization of Photoinduced Self-Exchange Reactions at Molecule-Semiconductor Interfaces by Transient Polarization Spectroscopy: Lateral Intermolecular Energy and Hole Transfer across Sensitized $TiO_2$ Thin Films. *J. Am. Chem. Soc.* **2011**, *133*, 15384−15396.
(31) Bonhôte, P.; Gogniat, E.; Tingry, S.; Barbé, C.; Vlachopoulos, N.; Lenzmann, F.; Comte, P.; Grätzel, M. Efficient Lateral Electron Transport inside a Monolayer of Aromatic Amines Anchored on Nanocrystalline Metal Oxide Films. *J. Phys. Chem. B* **1998**, *102*, 1498−1507.
(32) Trammell, S. A.; Meyer, T. J. Diffusional Mediation of Surface Electron Transfer on $TiO_2$. *J. Phys. Chem. B* **1999**, *103*, 104−107.
(33) Hu, K.; Meyer, G. J. Lateral Intermolecular Self-Exchange Reactions for Hole and Energy Transport on Mesoporous Metal Oxide Thin Films. *Langmuir* **2015**, *31*, 11164−11178.
(34) Moia, D.; Leijtens, T.; Noel, N.; Snaith, H. J.; Nelson, J.; Barnes, P. R. F. Dye Monolayers Used as the Hole Transporting Medium in Dye-Sensitized Solar Cells. *Adv. Mater.* **2015**, *27*, 5889−5894.
(35) Sampaio, R. N.; Dimarco, B. N.; Meyer, G. J. Activation Energies for Electron Transfer from $TiO_2$ to Oxidized Dyes: A Surface Coverage Dependence Correlated with Lateral Hole Hopping. *ACS Energy Lett.* **2017**, *2*, 2402−2407.
(36) Sampaio, R. N.; Müller, A. V.; Polo, A. S.; Meyer, G. J. Correlation between Charge Recombination and Lateral Hole-Hopping Kinetics in a Series of *cis*-Ru(Phen′)(dcb)$(NCS)_2$ Dye-Sensitized Solar Cells. *ACS Appl. Mater. Interfaces* **2017**, *9*, 33446−33454.
(37) Troian-Gautier, L.; DiMarco, B. N.; Sampaio, R. N.; Marquard, S. L.; Meyer, G. J. Evidence That S‡ Controls Interfacial Electron Transfer Dynamics from Anatase TiO2 to Molecular Acceptors. *J. Am. Chem. Soc.* **2018**, *140*, 3019−3029.
(38) Hanson, K.; Losego, M. D.; Kalanyan, B.; Ashford, D. L.; Parsons, G. N.; Meyer, T. J. Stabilization of $[Ru(bpy)_2(4,4'-(PO_3H_2)bpy)]^{2+}$ on Mesoporous $TiO_2$ with Atomic Layer Deposition of $Al_2O_3$. *Chem. Mater.* **2013**, *25*, 3−5.
(39) Kim, D. H.; Losego, M. D.; Hanson, K.; Alibabaei, L.; Lee, K.; Meyer, T. J.; Parsons, G. N. Stabilizing Chromophore Binding on $TiO_2$ for Long-Term Stability of Dye-Sensitized Solar Cells Using Multicomponent Atomic Layer Deposition. *Phys. Chem. Chem. Phys.* **2014**, *16*, 8615−8622.
(40) Son, H. J.; Kim, C. H.; Kim, D. W.; Jeong, N. C.; Prasittichai, C.; Luo, L.; Wu, J.; Farha, O. K.; Wasielewski, M. R.; Hupp, J. T. Post-Assembly Atomic Layer Deposition of Ultrathin Metal-Oxide Coatings Enhances the Performance of an Organic Dye-Sensitized Solar Cell by Suppressing Dye Aggregation. *ACS Appl. Mater. Interfaces* **2015**, *7*, 5150−5159.
(41) Lapides, A. M.; Sherman, B. D.; Brennaman, M. K.; Dares, C. J.; Skinner, K. R.; Templeton, J. L.; Meyer, T. J. Synthesis, Characterization, and Water Oxidation by a Molecular Chromophore-Catalyst Assembly Prepared by Atomic Layer Deposition. The "Mummy" Strategy. *Chem. Sci.* **2015**, *6*, 6398−6406.
(42) Wang, D.; Sheridan, M. V.; Shan, B.; Farnum, B. H.; Marquard, S. L.; Sherman, B. D.; Eberhart, M. S.; Nayak, A.; Dares, C. J.; Das, A. K.; Bullock, R. M.; Meyer, T. J. Layer-by-Layer Molecular Assemblies for Dye-Sensitized Photoelectrosynthesis Cells Prepared by Atomic Layer Deposition. *J. Am. Chem. Soc.* **2017**, *139*, 14518−14525.
(43) Eberhart, M. S.; Wang, D.; Sampaio, R. N.; Marquard, S. L.; Shan, B.; Brennaman, M. K.; Meyer, G. J.; Dares, C.; Meyer, T. J. Water Photo-Oxidation Initiated by Surface-Bound Organic Chromophores. *J. Am. Chem. Soc.* **2017**, *139*, 16248−16255.
(44) Kamire, R. J.; Materna, K. L.; Hoffeditz, W. L.; Phelan, B. T.; Thomsen, J. M.; Farha, O. K.; Hupp, J. T.; Brudvig, G. W.; Wasielewski, M. R. Photodriven Oxidation of Surface-Bound Iridium-Based Molecular Water-Oxidation Catalysts on Perylene-3,4-Dicarboximide-Sensitized $TiO_2$ Electrodes Protected by an $Al_2O_3$ Layer. *J. Phys. Chem. C* **2017**, *121*, 3752−3764.
(45) DiMarco, B. N.; Motley, T. C.; Balok, R. S.; Li, G.; Siegler, M. A.; O'Donnell, R. M.; Hu, K.; Meyer, G. J. A Distance Dependence to Lateral Self-Exchange across Nanocrystalline $TiO_2$. A Comparative Study of Three Homologous $Ru^{III/II}$ Polypyridyl Compounds. *J. Phys. Chem. C* **2016**, *120*, 14226−14235.
(46) Motley, T. C.; Brady, M. D.; Meyer, G. J. Influence of 4 and 4′ Substituents on $Ru^{III/II}$ Bipyridyl Self-Exchange Electron Transfer across Nanocrystalline $TiO_2$ Surfaces. *J. Phys. Chem. C* **2018**, *122*, 19385−19394.
(47) Heimer, T. A.; D'Arcangelis, S. T.; Farzad, F.; Stipkala, J. M.; Meyer, G. J. An Acetylacetonate-Based Semiconductor-Sensitizer Linkage. *Inorg. Chem.* **1996**, *35*, 5319−5324.
(48) Troian-Gautier, L.; Sampaio, R. N.; Piechota, E. J.; Brady, M. D.; Meyer, G. J. Barriers for Interfacial Back-Electron Transfer: A Comparison between $TiO_2$ and $SnO_2/TiO_2$ Core/Shell Structures. *J. Chem. Phys.* **2019**, *150*, No. 041719.
(49) Jur, J. S.; Parsons, G. N. Atomic Layer Deposition of $Al_2O_3$ and ZnO at Atmospheric Pressure in a Flow Tube Reactor. *ACS Appl. Mater. Interfaces* **2011**, *3*, 299−308.
(50) Argazzi, R.; Bignozzi, C. A.; Heimer, T. A.; Castellano, F. N.; Meyer, G. J. Enhanced Spectral Sensitivity from Ruthenium(II) Polypyridyl Based Photovoltaic Devices. *Inorg. Chem.* **1994**, *33*, 5741−5749.
(51) Ashford, D. L.; Brennaman, M. K.; Brown, R. J.; Keinan, S.; Concepcion, J. J.; Papanikolas, J. M.; Templeton, J. L.; Meyer, T. J. Varying the Electronic Structure of Surface-Bound Ruthenium(II) Polypyridyl Complexes. *Inorg. Chem.* **2015**, *54*, 460−469.
(52) Barbé, C. J.; Arendse, F.; Comte, P.; Jirousek, M.; Lenzmann, F.; Shklover, V.; Grätzel, M. Nanocrystalline Titanium Oxide Electrodes for Photovoltaic Applications. *J. Am. Ceram. Soc.* **1997**, *80*, 3157−3171.
(53) Moia, D.; Vaissier, V.; López-Duarte, I.; Torres, T.; Nazeeruddin, M. K.; O'Regan, B. C.; Nelson, J.; Barnes, P. R. F. The Reorganization Energy of Intermolecular Hole Hopping between Dyes Anchored to Surfaces. *Chem. Sci.* **2014**, *5*, 281−290.
(54) Blauch, D. N.; Savéant, J. M. Dynamics of Electron Hopping in Assemblies of Redox Centers. Percolation and Diffusion. *J. Am. Chem. Soc.* **1992**, *114*, 3323−3332.
(55) Bergeron, B. V.; Kelly, C. A.; Meyer, G. J. Thin Film Actinometers for Transient Absorption Spectroscopy: Applications to Dye-Sensitized Solar Cells. *Langmuir* **2003**, *19*, 8389−8394.
(56) Grätzel, M. Solar Energy Conversion by Dye-Sensitized Photovoltaic Cells. *Inorg. Chem.* **2005**, *44*, 6841−6851.
(57) Hanson, K.; Brennaman, M. K.; Ito, A.; Luo, H.; Song, W.; Parker, K. A.; Ghosh, R.; Norris, M. R.; Glasson, C. R. K.; Concepcion, J. J.; Lopez, R.; Meyer, T. J. Structure-Property Relationships in Phosphonate-Derivatized, $Ru^{II}$ Polypyridyl Dyes on Metal Oxide Surfaces in an Aqueous Environment. *J. Phys. Chem. C* **2012**, *116*, 14837−14847.
(58) Zigler, D. F.; Morseth, Z. A.; Wang, L.; Ashford, D. L.; Brennaman, M. K.; Grumstrup, E. M.; Brigham, E. C.; Gish, M. K.; Dillon, R. J.; Alibabaei, L.; Meyer, G. J.; Meyer, T. J.; Papanikolas, J. M. Disentangling the Physical Processes Responsible for the Kinetic Complexity in Interfacial Electron Transfer of Excited Ru(II) Polypyridyl Dyes on TiO2. *J. Am. Chem. Soc.* **2016**, *138*, 4426−4438.
(59) Lakowicz, J. R. *Principles of Fluorescence Spectroscopy*; Springer: New York, 2006.
(60) Terpetschnig, E.; Szmacinski, H.; Malak, H.; Lakowicz, J. R. Metal-Ligand Complexes as a New Class of Long-Lived Fluorophores for Protein Hydrodynamics. *Biophys. J.* **1995**, *68*, 342−350.
(61) Wallin, S.; Davidsson, J.; Modin, J.; Hammarström, L. Femtosecond Transient Absorption Anisotropy Study on $[Ru(bpy)_3]^{2+}$ and $[Ru(bpy)(py)_4]^{2+}$·Ultrafast Interligand Randomization of the MLCT State. *J. Phys. Chem. A* **2005**, *109*, 4697−4704.
(62) Wallin, S.; Davidsson, J.; Modin, J.; Hammarström, L. Femtosecond Transient Absorption Anisotropy Study on [Ru-


DOI: 10.1021/acsami.9b08051
ACS Appl. Mater. Interfaces 2019, 11, 27453−27463

$(bpy)_3]^{2+}$ and $[Ru(bpy)(py)_4]^{2+}$· Ultrafast Interligand Randomization of the MLCT State. *J. Phys. Chem. A* **2005**, *109*, 9378.
(63) Chen, P.; Meyer, T. J. Electron Transfer in Frozen Media. *Inorg. Chem.* **1996**, *35*, 5520−5524.
(64) Gaines, G. L., III; O'Neill, M. P.; Svec, W. A.; Niemczyk, M. P.; Wasielewski, M. R. Photoinduced Electron Transfer in the Solid State: Rate vs Free Energy Dependence in Fixed-Distance Porphyrin-Acceptor Molecules. *J. Am. Chem. Soc.* **1991**, *113*, 719−721.
(65) Meyer, T. J.; Sheridan, M. V.; Sherman, B. D. Mechanisms of Molecular Water Oxidation in Solution and on Oxide Surfaces. *Chem. Soc. Rev.* **2017**, *46*, 6148−6169.
(66) Motley, T. C.; Meyer, G. J. Intramolecular Electronic Coupling Enhances Lateral Electron Transfer across Semiconductor Interfaces. *J. Phys. Chem. C* **2018**, *122*, 14420−14424.



DOI: 10.1021/acsami.9b08051
*ACS Appl. Mater. Interfaces* 2019, 11, 27453−27463